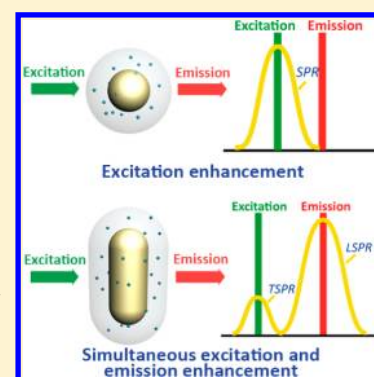


Simultaneous Excitation and Emission Enhancement of Fluorescence Assisted by Double Plasmon Modes of Gold Nanorods

Si-Yun Liu, Lu Huang, Jia-Fang Li,* Chen Wang, Qiang Li, Hong-Xing Xu, Hong-Lian Guo, Zi-Ming Meng, Zhe Shi, and Zhi-Yuan Li*

Beijing National Laboratory for Condensed Matter Physics, Institute of Physics, Chinese Academy of Sciences, Beijing 100190, China

ABSTRACT: Here we propose a scheme utilizing the double plasmon modes of gold nanorod (GNR) to efficiently enhance the fluorescence of surrounding emitters. The transversal and longitudinal surface plasmon resonance (TSPR and LSPR, respectively) modes of GNR are simultaneously utilized to enhance the excitation and emission efficiency, respectively. To demonstrate the idea, GNRs coated with an Oxazine-725 dye molecule-doped silica shell are employed. For comparison, gold nanospheres with the same shell are also studied, of which the single plasmon resonance mode matches only with the excitation wavelength of Oxazine-725. The experimental results, in agreement with theoretical simulations using the discrete dipole approximation method, successfully demonstrate the efficient excitation and emission enhancement of fluorescence assisted by the double SPRs of GNRs.



INTRODUCTION

Metal nanoparticles exhibit fascinating plasmonic properties with potential applications ranging from bioscience, catalysis, and sensing to information technology uses such as imaging and storage. The excitation of localized surface plasmon resonance (SPR) in metal nanoparticles results in the nanoscale confinement of electromagnetic fields near the metal surface and a significant enhancement in the local density of optical states.^{1–5} These properties have been widely employed to study the interactions between plasmons and fluorophores, such as fluorescence enhancement^{6–15} and the realization of a nanolaser.^{16–20} In principle, for the plasmon-enhanced fluorescence, there are two kinds of enhancement mechanisms: excitation enhancement^{6,21,22} and emission enhancement.^{6,21}

Although utilization of a single SPR of some metal nanoparticles can result in either excitation enhancement or emission enhancement, many experimental results have shown that for maximum “excitation–emission” efficiency, the SPR wavelength lies between the peak excitation wavelength and peak emission wavelength of the emitters, as schematically illustrated in Figure 1a.^{7,21} Such compromised phenomena are frequently seen in SERS experiments as well.^{23,24} The essence of this phenomenon is that the excitation–emission efficiency, η , of fluorescence molecules is related simultaneously to the excitation efficiency, γ_{Ex} and the emission efficiency, γ_{Em} ,^{25–27} and can be simply described as $\eta = \gamma_{\text{Ex}}\gamma_{\text{Em}}$. The excitation wavelength of lasers and the emission wavelength of fluorescence molecules are described as λ_{Ex} and λ_{Em} , respectively. When the SPR wavelength of the metal particle satisfies the relation $\lambda_{\text{SPR}} = \lambda_{\text{Ex}}$, the highest excitation efficiency, $(\gamma_{\text{Ex}})_{\text{max}}$, is achieved. If $\lambda_{\text{SPR}} = \lambda_{\text{Em}}$, the highest emission efficiency, $(\gamma_{\text{Em}})_{\text{max}}$, is achieved. However, generally, because $\lambda_{\text{Em}} \neq \lambda_{\text{Ex}}$ if λ_{SPR} matches one of the wavelengths, the other

must be mismatched. Therefore, $(\gamma_{\text{Ex}})_{\text{max}}$ and $(\gamma_{\text{Em}})_{\text{max}}$ cannot be accomplished simultaneously. If $\lambda_{\text{Ex}} < \lambda_{\text{SPR}} < \lambda_{\text{Em}}$, the line width of the SPR spectrum can encompass both the excitation and emission bands of fluorescence molecules and thus result in an optimized but compromised excitation–emission efficiency η_{Com} . Obviously, $\eta_{\text{Com}} < (\gamma_{\text{Ex}})_{\text{max}}(\gamma_{\text{Em}})_{\text{max}}$.

Here we present a scheme to further increase the excitation–emission efficiency. By matching the double SPR wavelengths (transversal and longitudinal SPR modes) with the excitation and emission wavelengths, respectively, one can realize $(\gamma_{\text{Ex}})_{\text{max}}$ and $(\gamma_{\text{Em}})_{\text{max}}$ simultaneously and achieve $\eta_{\text{max}} = (\gamma_{\text{Ex}})_{\text{max}}(\gamma_{\text{Em}})_{\text{max}}$. The proposed idea is implemented using a gold nanorod (GNR) encapsulated in a fluorophore-doped silica shell, which has two SPR modes, as shown in Figure 1b. Compared with various experimental samples, the proposed hybrid GNR structure shows the highest fluorescence intensity, which is ~ 20 and ~ 4 times the corresponding emission from the same amount of dye molecules in solution and in a gold nanosphere (GNS) sample, respectively. The results are further confirmed by time-resolved measurements using a time-correlated single-photon counting (TCSPC) technique and by numerical simulations using the discrete dipole approximation (DDA) method.

EXPERIMENTAL SECTION

Sample Preparation and Characterization. Samples of gold nanoparticles coated with an Oxazine-725-doped silica shell were customized and commercially obtained from Nanoseedz company in water solution.⁶ Three ensemble

Received: January 5, 2013

Revised: April 1, 2013

Published: April 29, 2013

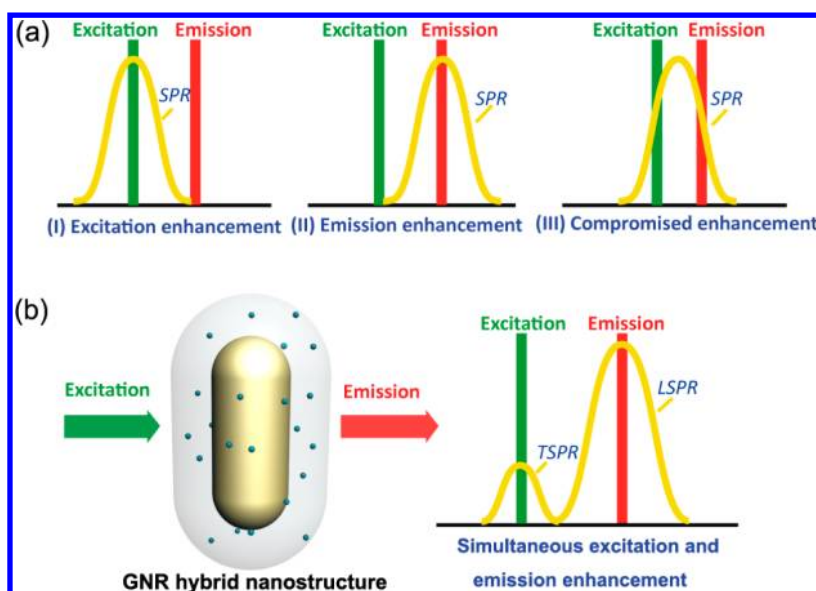


Figure 1. Schematic models of the fluorescence enhancement mechanisms assisted by the SPR of metal nanoparticles. (a) The excitation enhancement (I) and emission enhancement (II) are realized by matching the single SPR wavelength with the excitation and emission wavelength, respectively. Optimized but compromised enhancement (III) is generally achieved by overlapping the single SPR band with both the excitation and emission wavelengths. (b) Simultaneous excitation and emission enhancement utilizing the transversal surface plasmon resonance (TSPR) mode of gold nanorods to enhance the excitation possibility and the longitudinal surface plasmon resonance (LSPR) mode to enhance the emission rate.

samples were used in experiments: (a) hybrid GNS with an SPR wavelength of 543 nm (labeled as GNS), (b) hybrid GNRs with an LSPR wavelength of 739 nm (labeled as Sample 1), and (c) hybrid GNRs with an LSPR wavelength of 877 nm (labeled as Sample 2). To obtain a similar number of Oxazine-725 molecules in the silica shells of different samples, the same amount of Oxazine-725 molecules and other chemicals were added during the synthesis, resulting in the same concentration of fluorophore molecules (~ 11 per 1000 nm^3) in the silica shells. Under such conditions, the number of fluorophore molecules in each nanoparticle was obtained by multiplying the concentration of fluorophore molecules with the volume of the silica shell, the dimensions of which were obtained by high-resolution SEM characterizations. For the characterizations, GNS, Sample 1, and Sample 2 in water solutions were deposited onto ITO glass slides, and the sample areas were then covered by copper grids for position recognition. With this preparation, fast and high-resolution SEM characterizations can be conducted without jeopardizing the nanoparticles. To conduct the single-nanoparticle experiments, three kinds of well-separated single nanoparticles named GNS1, GNR1, and GNR2 were chosen from the deposited samples on ITO glass slides. SEM characterization of the samples was performed with an electron beam lithography system (Raith 150) working in back-scattering mode.

Spectral Measurement. Absorbance spectra of the samples in water solution were measured using an optical spectrometer (Ocean Optics, QE65000) and tungsten halogen light sources (Ocean Optics, HL-2000). In order to measure the scattering and emission from exactly the same single nanoparticles, a dark-field (DF) scattering microscope (Leica, DMIRB) combined with a photoluminescence measurement system was employed. The DF scattering was excited by a white-light lamp, and the fluorescence was excited by a focused continuous 532 nm laser. Both the DF scattering and fluorescence spectra of a single nanoparticle were collected with the same objective (Olympus, NA = 0.9, 100 \times) and then

measured with an optical spectrometer (Ocean Optics, QE65000).

Lifetime Measurement. Fluorescence intensity decays of the samples were measured using a time-correlated single-photon counting (TCSPC) system, in which a 532 nm pulsed laser (PicoQuant, LDH-D-C-485, controlled by a PDL-800B driver; laser power = 2.5 mW; repetition rate = 10 MHz; pulse width = 78 ps) was used. The laser light was focused onto the sample, and the emission was collected by the same objective (Olympus, NA = 0.9, $\times 100$). Spatial filtering was realized by a confocal lens with a pinhole (diameter = 100 μm) in the center, which enables light collection from an area as small as 1 μm in diameter on the sample's surface. The collected fluorescence was coupled to a single-photon counting avalanche photodiode (PicoQuant, MPD) after passing a 590 nm long-pass filter, and the lifetime measurement was carried out using a TCSPC module (PicoQuant, PicoHarp 300). The instrument response time was about 200 ps.

THEORETICAL SECTION

Numerical simulations are carried out using the DDA method.^{28–30} The core–shell GNS in simulation has a gold sphere (named GNS1_C) with a diameter of 64 nm in the core and a uniform 23 nm-thick silica shell. The GNR is modeled as a cylinder capped with two hemispheres at each end. GNRs with different sizes and aspect ratios (AR) are modeled. One is 44 nm in diameter and 96 nm in length (named GNR1_C, AR = 2.2), while the other is 12 nm in diameter and 36 nm in length (named GNR2_C, AR = 3). They are coated by silica shells with the same uniform thickness of 23 nm and a refractive index of 1.5. These hybrid nanostructures are surrounded by air with a refractive index of 1.0. Each Oxazine-725 molecule is modeled as a single dipole. The fluorescence enhancement factor is calculated in two steps. First, the linearly polarized incident wave of 532 nm excites the localized SPR of the core–shell nanoparticle and the fluorophore dipole, resulting in near-field enhancement around the metal nanoparticle. Because the

excitation probability of the fluorophore is proportional to the local electric field, the excitation enhancement factor can be defined as the near-field enhancement at the position of the fluorophore dipole, which is described as $\gamma_{\text{Ex}} = |\mathbf{E}_{\text{d}}|^2 / |\mathbf{E}_0|^2$. Here, $|\mathbf{E}_{\text{d}}|^2$ and $|\mathbf{E}_0|^2$ describe the intensity of total electric field and incident field at the position of fluorophore, respectively. Second, via substitution of the incident plane wave in the first step, the fluorophore dipole then acts as a dipole source with a working wavelength of 692 nm that is ideally matched with the LSPR wavelength of the core-shell GNR1_C. The emission enhancement factor is described as $\gamma_{\text{Em}} = C_{\text{scat}} / C_{\text{scat}0}$, where C_{scat} and $C_{\text{scat}0}$ stand for the total scattering cross section in the presence and absence of the core-shell nanoparticle in the system, respectively. The scattering cross section is calculated from eq 1.²⁸

$$C_{\text{scat}} = \frac{k^4}{|\mathbf{E}_{\text{inc}}|^2} \int d\Omega \left| \sum_{j=1}^N [\mathbf{P}_j - \hat{\mathbf{n}}(\hat{\mathbf{n}} \cdot \mathbf{P}_j)] \exp(-ik\hat{\mathbf{n}} \cdot \mathbf{r}_j) \right|^2 \quad (1)$$

where \mathbf{E}_{inc} is the electric field of the incident source, $k = \lambda/2\pi$ with λ being the wavelength of the incident radiation, \mathbf{P}_j the dipole moment of the j th dipole, \mathbf{r}_j the directional vector between the j th dipole and the origin of the simulation space, $\hat{\mathbf{n}}$ the unit vector in the direction of the scattering, and $d\Omega$ the element of the solid angle. The averaged emission enhancement factor, $\gamma_{\text{Em-avg}}$, is then obtained by averaging the enhancement factors resulting from the fluorophore dipole moments along x -, y -, and z -axes (the long axis of a GNR is along the z -axis) by considering the random molecule dipole moment. Finally, the averaged total fluorescence enhancement factor, η_{avg} is calculated using $\eta_{\text{avg}} = \gamma_{\text{Ex-avg}} \gamma_{\text{Em-avg}}$.

RESULTS AND DISCUSSION

Our experiments were based on hybrid nanostructures composed of GNRs or GNS in the core and Oxazine-725-doped silica in the shell (see Experimental Section), which have been utilized for studies on plasmon-enhanced fluorescence and plasmon-molecule interactions.^{7,21,31} Because fluorescence can be chemically quenched when fluorophores are located very close (<5 nm) to the metal surface,^{21,32–38} the thickness of the silica shell in our studies was chosen to be around 20 nm, with which a net fluorescence enhancement can be measured. Wavelength matching is critical when testing the proposed fluorescence enhancement effects induced by the double SPRs of GNRs. The excitation wavelength was chosen to be 532 nm, which is outside the emission band of Oxazine-725 (ranging from 600 to 800 nm, Figure 2a), to avoid an overlap between the excitation wavelength of the laser and the emission band of the molecules. The investigated GNR (named Sample 1) was chosen to have the transversal SPR (TSPR) and longitudinal SPR (LSPR) wavelength ranges overlap the excitation wavelength and the emission band, respectively, as shown in Figure 2a. It should be mentioned that the absorption spectra in Figure 2a were measured with a GNR solution, so they are averaged absorbance from a group of GNRs. In the following studies, a single GNR will be picked to have the LSPR peak matched exactly with the emission band of Oxazine-725. For comparison, GNSs were chosen with the single SPR wavelength matched with the excitation wavelength, so excitation enhancement is expected. Meanwhile, another GNR sample (named Sample 2) was chosen with double SPRs that

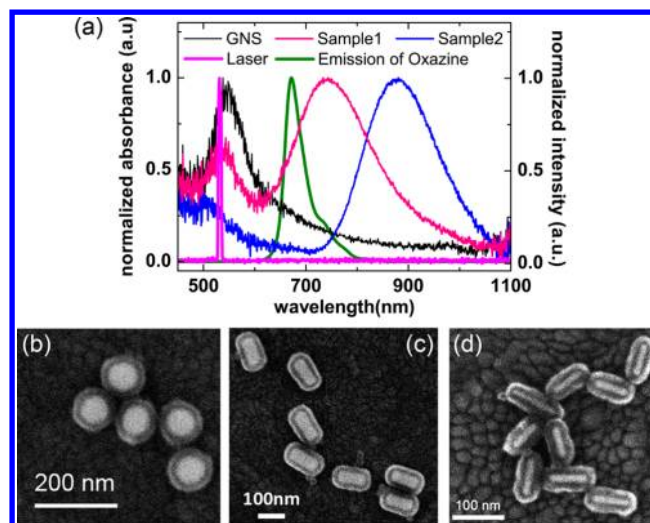


Figure 2. (a) (left) Absorbance spectra for the water solution of core-shell GNS, core-shell Sample 1, and core-shell Sample 2. (right) The spectrum of excitation laser and the emission spectrum of Oxazine-725 in water solution. (b–d) SEM images of group core-shell GNS, Sample 1, and Sample 2 on ITO glass slides.

overlapped neither with the excitation wavelength nor with the emission band of the dye molecules, as shown in Figure 2a.

To compare the fluorescence enhancement induced by the different mechanisms depicted in Figure 1, three types of single nanoparticles were selected by depositing the diluted sample solution (Figure 2) onto ITO glass slides (see Experimental Section). The three types were as follows: (1) GNS1, which had single SPR wavelength matched with the excitation wavelength (532 nm); (2) GNR1, whose TSPR and LSPR wavelengths were matched with the excitation wavelength and emission band of Oxazine-725, respectively; and (3) GNR2, which had SPRs matched neither with the excitation wavelength nor with the emission band. In order to measure the scattering and emission from exactly the same single nanoparticle, a combined DF scattering and photoluminescence characterization system was employed, as depicted in Figure 3 (see Experimental Section). Figure 4a shows the DF scattering and fluorescence spectra from a single core-shell GNS (named GNS1) whose SEM image is shown in the inset. The diameter of the core is 69 ± 5 nm, and the silica shell is uniform with a thickness of 23 ± 1 nm. By multiplying the volume of the silica

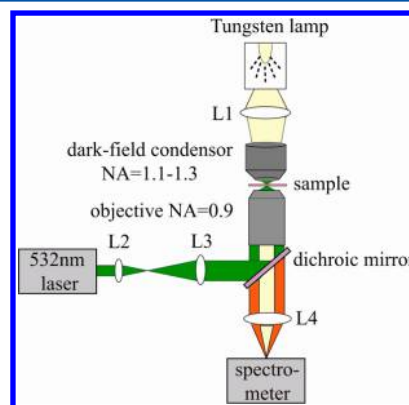


Figure 3. Schematic setup of the optical system for the single-particle dark-field scattering and fluorescence measurement. L1–L4 are optical lenses.

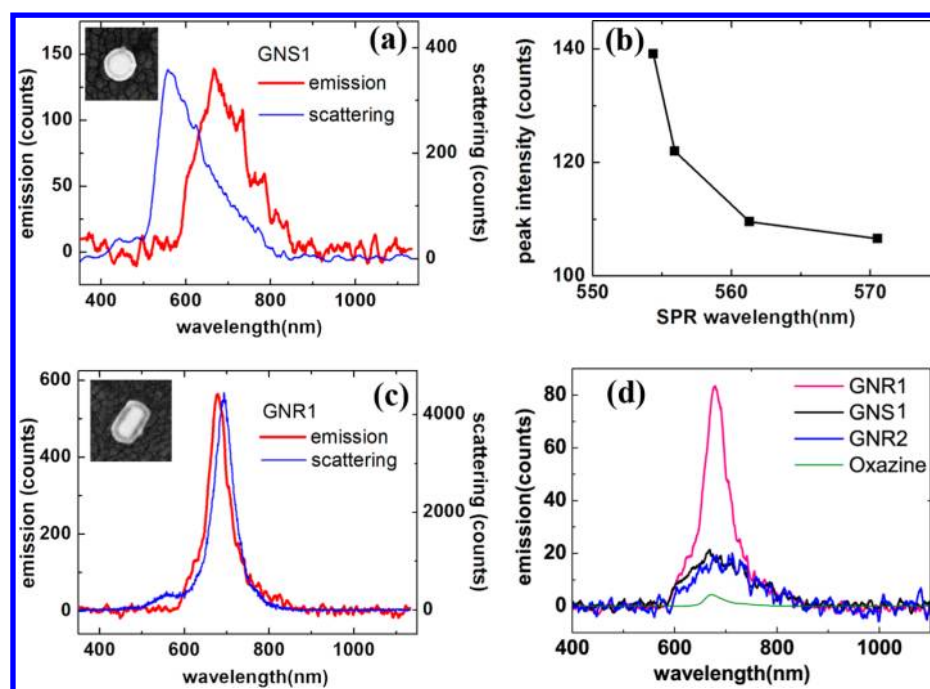


Figure 4. (a) Dark-field scattering spectrum and fluorescence spectrum of GNS1; SEM image of GNS1 shown in the inset. (b) Peak fluorescence intensity as a function of SPR wavelength for core–shell GNS with different sizes. The diameter of the GNS in the core (from left to right corresponding to the SPR wavelength) is about 65, 66, 68, and 70 nm, which was obtained from SEM characterizations. (c) Dark-field scattering spectrum and fluorescence spectrum of GNR1; SEM image of GNR1 is shown in the inset. (d) Fluorescence emission spectra (from top to bottom) of GNR1, GNS1, GNR2, and Oxazine-725 water solution. The spectra are recalculated from direct measurements and equivalently show the emission from the same number (1000) of dye molecules in each sample. The peak fluorescence intensities are 83, 21, 18, and 4 counts, for sample GNR1, GNS1, GNR2, and Oxazine-725 molecules in water solution, respectively.

shell with the given concentration of fluorophore molecules in the shell (~ 11 molecules per 1000 nm^3), we calculated the number of packed Oxazine-725 molecules in GNS1 to be ~ 6800 . As seen from Figure 4a, the DF scattering spectrum of GNS1 is centered at a wavelength of 554 nm, whereas the peak of the fluorescence spectra is at a wavelength of 666 nm when excited by the 532 nm laser. It is found that when a GNS with a different size is used, the peak fluorescence intensity from the core–shell GNS varies with its SPR wavelength, as shown in Figure 4b. One can see that the peak fluorescence intensity decreases when the SPR wavelength moves away from the excitation wavelength of the laser, which is a clear indication of the excitation enhancement as illustrated in Figure 1a.

In order to test our idea of utilizing the double SPR modes of GNRs to realize the excitation enhancement and emission enhancement simultaneously, a core–shell GNR labeled as GNR1 was studied, as shown in the inset of Figure 4c. This particle was chosen from Sample 1 deposited on an ITO glass slide. The GNR in the core is 100 ± 4 nm in length and 44 ± 2 nm in diameter, and the silica shell has a uniform thickness of 23 ± 1 nm. According to the calculated volume of the silica shell, there are about 6700 Oxazine-725 molecules packed into the silica shell of GNR1, which is at the same level as that of GNS1. As seen from Figure 4c, the peak scattering wavelength for GNR1 was measured at 693 nm, which originated from the LSPR mode. Because the TSPR mode was too weak to be detected by the DF measurement, it was estimated from the absorbance spectrum of Sample 1 (Figure 2a) to be around 530 nm. With such TSPR and LSPR wavelengths matched with the excitation wavelength (532 nm) and emission band (with fwhm from 660 to 702 nm) of Oxazine-725, the fluorescence intensity from GNR1 is strongly enhanced, as shown in Figure 4c. To

relatively quantify the emission enhancement effect, a core–shell GNR selected from Sample 2 deposited on ITO glass slide (named GNR2) was also studied. The core of GNR2 is 11 ± 3 nm in diameter and 43 ± 2 nm in length, while the silica shell is 20 ± 2 nm in thickness. With such dimensions, the number of packed fluorophore molecules in the silica shell is about 1400. Because the TSPR and LSPR wavelengths are around 500 and 830 nm, respectively, which are matched neither with the excitation wavelength nor with the emission band of Oxazine-725, no enhancement is expected from the fluorescence measurement. To compare the fluorescence intensity from various samples, the measured fluorescence spectra of GNS1, GNR1, GNR2, and Oxazine-725 molecules in solution are plotted in Figure 4d, with all spectra recalculated to show corresponding emission from the same number (1000) of fluorophore molecules. One can clearly see that GNR1, which has double SPRs matched with both excitation wavelength and emission band, has the strongest fluorescence. Compared with the emission from the same amount of dye molecules in solution, the peak fluorescence intensities from GNR1, GNS1, and GNR2 have been enhanced by 20.8, 5.3, and 4.5 times, respectively.

The relative enhanced emission from GNR samples was confirmed by conducting time-resolved experiments with a TCSPC system (see Experimental Section). Figure 5 shows the measured fluorescence intensity decays of Oxazine-725 in silica composite, GNS shell (with SPR wavelength at ~ 550 nm), and GNR shell (with LSPR wavelength at ~ 700 nm) with resolved lifetimes of 2.51, 1.46, and 0.72 ns, respectively. The shortest lifetime of Oxazine-725 molecules in GNR shell indicates that the emission rate at the LSPR wavelength is greatly enhanced, which is physically caused by the increased local densities of

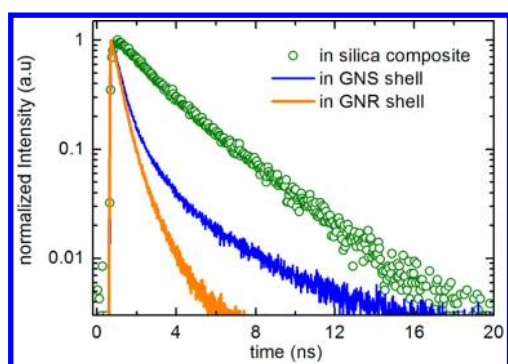


Figure 5. Measured fluorescence intensity decays of Oxazine-725 molecules in different samples as noted. It can be seen that fluorescence intensity in the GNR sample decays much faster than those in other samples.

optical states around GNR because of the existence of LSPR. It should be mentioned that the decrease in lifetime is not as great as the increase in peak fluorescence intensity (Figure 4d). This is because the measured fluorescence intensity decays in Figure 5 were from the whole emission band of Oxazine-725 rather than at only the peak wavelength.

To verify the experimental observations, numerical simulations are carried out using the DDA method (see Theoretical Section). The size used in the simulations is based on the SEM images of each nanostructure as illustrated in Figures 2b–d and 4. In this case, the theoretical studies can largely simulate the real situations. As shown in Figure 6, the calculated SPR

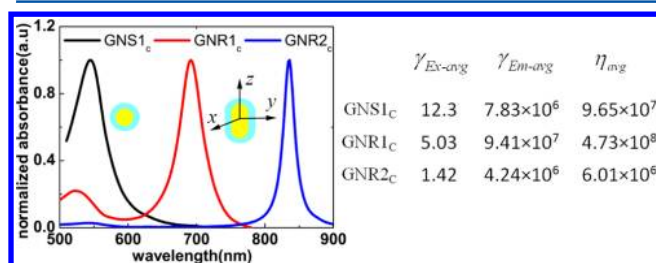


Figure 6. Calculated scattering spectra for the core-shell GNS1_c, GNR1_c, and GNR2_c, the peak SPR wavelengths of which are 558, 692, and 836 nm, respectively. The calculated total fluorescence enhancement factors (averaged, η_{avg}) for the three kinds of nanostructures are noted at the right.

wavelength for silica-coated GNS1 (named GNS1_c) is 558 nm, while the calculated LSPR wavelengths for the silica-coated GNR1 (named GNR1_c) and GNR2 (named GNS2_c) are 692 and 836 nm, respectively. On the basis of a two-step simulation (see Theoretical Section), the averaged excitation and emission enhancement factors for the core-shell GNS and core-shell GNRs were calculated and are summarized in Figure 6, where the averaged total fluorescence enhancement factor η_{avg} was given by $\eta_{avg} = \gamma_{Ex-avg} \gamma_{Em-avg}$. It can be seen that $\eta_{avg-GNR1c} > \eta_{avg-GNS1c} > \eta_{avg-GNR2c}$. It clearly demonstrates that the double SPR enhancement scheme is superior to the simple excitation enhancement scheme, both of which are better than the situation where SPR does not enhance either the excitation or the emission.

It should be mentioned that our experimental results show smaller enhancement effects than those of the simulations. This can be attributed to four factors. First, in the simulations, the

fluorophore dipole is located near the end of three gold nanoparticles in the core with a short distance of 3 nm, while the experimental conditions contain randomly distributed fluorophores and quenching effects, which attenuate the enhancement effects. Second, because of depolarization effects in experiments, the polarization-dependent excitation and emission effects^{6,31,39–42} are largely averaged in measurement, which also causes a decrease in enhancement effects. Third, the refractive index of Oxazine-725-doped silica used in simulations, which is used to phenomenologically describe the response of the fluorophore to the light, might be different from the real conditions. Last but not least, the simulated results reflect the near-field interactions, the features of which cannot be fully represented in the far-field spectra. Nevertheless, our experimental results demonstrate the feasibility of utilizing the double SPRs of GNRs for simultaneous excitation and emission enhancement.

CONCLUSIONS

In conclusion, we have proposed and demonstrated an effective scheme to enhance fluorescence utilizing the double SPR modes of GNRs. In this scheme, the excitation probability of the dye molecules is first enhanced by the local electric field enhancement because of the TSPR of the GNR. Then the emission rate at the LSPR wavelength is further enhanced by the increased local densities of optical states around GNR because of the existence of LSPR. From the other aspect, the GNR acts as a nanoantenna in the process of emission enhancement.^{43–46} By experimentally employing GNRs coated with a dye molecule-doped silica shell, the maximum fluorescence enhancement factor is obtained when the TSPR and LSPR wavelengths of GNR are well-matched with the excitation wavelength and emission band of dye molecules, respectively. The experimental observations are further confirmed by numerical simulations with the DDA method. Our scheme has opened up a new way toward enhancing the fluorescence or SERS signals by fully utilizing the multiple SPRs of plasmonic nanostructures.

AUTHOR INFORMATION

Corresponding Author

*J.-F.L.: jiafangli@aphy.iphy.ac.cn. Z.-Y.L.: lizy@aphy.iphy.ac.cn.

Notes

The authors declare no competing financial interest.

ACKNOWLEDGMENTS

This work was supported by the 973 Program of China (2013CB632704 and 2013CB922404), the Knowledge Innovation Project of CAS (Grant KJCX2-EW-W02), and the National Natural Science Foundation of China under Grant 11104342. We thank Dr. Tian Ming for the kind discussions of sample preparations.

REFERENCES

- (1) Martin, O. J. F.; Girard, C.; Dereux, A. Generalized Field Propagator for Electromagnetic Scattering and Light Confinement. *Phys. Rev. Lett.* **1995**, *74* (4), 526–529.
- (2) Hohenester, U.; Ditlbacher, H.; Krenn, J. R. Electron-Energy-Loss Spectra of Plasmonic Nanoparticles. *Phys. Rev. Lett.* **2009**, *103*, 106801.

- (3) Frimmer, M.; Coenen, T.; Koenderink, A. F. Signature of a Fano Resonance in a Plasmonic Metamolecule's Local Density of Optical States. *Phys. Rev. Lett.* **2012**, *108*, 077404.
- (4) Wiley, B. J.; Im, S. H.; Li, Z. Y.; McLellan, J.; Siekkinen, A.; Xia, Y. N. Maneuvering the Surface Plasmon Resonance of Silver Nanostructures through Shape-Controlled Synthesis. *J. Phys. Chem. B* **2006**, *110* (32), 15666–15675.
- (5) Hu, M.; Chen, J. Y.; Li, Z. Y.; Au, L.; Hartland, G. V.; Li, X. D.; Marquez, M.; Xia, Y. N. Gold Nanostructures: Engineering Their Plasmonic Properties for Biomedical Applications. *Chem. Soc. Rev.* **2006**, *35* (11), 1084–1094.
- (6) Ming, T.; Zhao, L.; Yang, Z.; Chen, H. J.; Sun, L. D.; Wang, J. F.; Yan, C. H. Strong Polarization Dependence of Plasmon-Enhanced Fluorescence on Single Gold Nanorods. *Nano Lett.* **2009**, *9* (11), 3896–3903.
- (7) Chen, Y.; Munechika, K.; Ginger, D. S. Dependence of Fluorescence Intensity on the Spectral Overlap between Fluorophores and Plasmon Resonant Single Silver Nanoparticles. *Nano Lett.* **2007**, *7* (3), 690–696.
- (8) Yang, Z.; Ni, W. H.; Kou, X. S.; Zhang, S. Z.; Sun, Z. H.; Sun, L. D.; Wang, J. F.; Yan, C. H. Incorporation of Gold Nanorods and Their Enhancement of Fluorescence in Mesoporous Silica Thin Films. *J. Phys. Chem. C* **2008**, *112* (48), 18895–18903.
- (9) Wang, J. T.; Moore, J.; Lailue, S.; Nantz, M.; Achilefu, S.; Kang, K. A. Fluorophore-Gold Nanoparticle Complex for Sensitive Optical Biosensing and Imaging. *Nanotechnology* **2012**, *23*, 095501.
- (10) Zhang, T. Y.; Lu, G. W.; Li, W. Q.; Liu, J.; Hou, L.; Perriat, P.; Martini, M.; Tillement, O.; Gong, Q. H. Optimally Designed Nanoshell and Matryoshka-Nanoshell as a Plasmonic-Enhanced Fluorescence Probe. *J. Phys. Chem. C* **2012**, *116* (15), 8804–8812.
- (11) Fu, Y.; Zhang, J.; Lakowicz, J. R. Plasmon-Enhanced Fluorescence from Single Fluorophores End-Linked to Gold Nanorods. *J. Am. Chem. Soc.* **2010**, *132* (16), 5540–5541.
- (12) Stranik, O.; McEvoy, H. M.; McDonagh, C.; MacCraith, B. D. Plasmonic Enhancement of Fluorescence for Sensor Applications. *Sens. Actuators, B* **2005**, *107* (1), 148–153.
- (13) Tam, F.; Goodrich, G. P.; Johnson, B. R.; Halas, N. J. Plasmonic Enhancement of Molecular Fluorescence. *Nano Lett.* **2007**, *7* (2), 496–501.
- (14) Bardhan, R.; Grady, N. K.; Cole, J. R.; Joshi, A.; Halas, N. J. Fluorescence Enhancement by Au Nanostructures: Nanoshells and Nanorods. *ACS Nano* **2009**, *3* (3), 744–752.
- (15) Schuller, J. A.; Barnard, E. S.; Cai, W. S.; Jun, Y. C.; White, J. S.; Brongersma, M. L. Plasmonics for Extreme Light Concentration and Manipulation. *Nat. Mater.* **2010**, *9* (3), 193–204.
- (16) Stockman, M. I. The Spaser as a Nanoscale Quantum Generator and Ultrafast Amplifier. *Journal of Optics (UK)* **2010**, *12*, 024004.
- (17) Oulton, R. F.; Sorger, V. J.; Zentgraf, T.; Ma, R. M.; Gladden, C.; Dai, L.; Bartal, G.; Zhang, X. Plasmon Lasers at Deep Subwavelength Scale. *Nature* **2009**, *461* (7264), 629–632.
- (18) Berini, P.; De Leon, I. Surface Plasmon-Polariton Amplifiers and Lasers. *Nat. Photonics* **2012**, *6* (1), 16–24.
- (19) Liu, S. Y.; Li, J. F.; Zhou, F.; Gan, L.; Li, Z. Y. Efficient Surface Plasmon Amplification from Gain-Assisted Gold Nanorods. *Opt. Lett.* **2011**, *36* (7), 1296–1298.
- (20) Noginov, M. A.; Zhu, G.; Belgrave, A. M.; Bakker, R.; Shalae, V. M.; Narimanov, E. E.; Stout, S.; Herz, E.; Suteewong, T.; Wiesner, U. Demonstration of a Spaser-Based Nanolaser. *Nature* **2009**, *460* (7259), 1110–U68.
- (21) Chen, H. J.; Ming, T. A.; Zhao, L.; Wang, F.; Sun, L. D.; Wang, J. F.; Yan, C. H. Plasmon-Molecule Interactions. *Nano Today* **2010**, *5* (5), 494–505.
- (22) Li, X.; Kao, F. J.; Chuang, C. C.; He, S. L. Enhancing Fluorescence of Quantum Dots by Silica-Coated Gold Nanorods under One- and Two-Photon Excitation. *Opt. Express* **2010**, *18* (11), 11335–11346.
- (23) Haynes, C. L.; Van Duyne, R. P. Plasmon-Sampled Surface-Enhanced Raman Excitation Spectroscopy. *J. Phys. Chem. B* **2003**, *107* (30), 7426–7433.
- (24) Willets, K. A.; Van Duyne, R. P. Localized Surface Plasmon Resonance Spectroscopy and Sensing. *Annu. Rev. Phys. Chem.* **2007**, *58*, 267–297.
- (25) Liaw, J. W.; Tsai, H. Y. Theoretical Investigation of Plasmonic Enhancement of Silica-Coated Gold Nanorod on Molecular Fluorescence. *J. Quant. Spectrosc. Radiat. Transfer* **2012**, *113* (6), 470–479.
- (26) Ming, T.; Chen, H. J.; Jiang, R. B.; Li, Q.; Wang, J. F. Plasmon-Controlled Fluorescence: Beyond the Intensity Enhancement. *J. Phys. Chem. Lett.* **2012**, *3* (2), 191–202.
- (27) Kang, K. A.; Wang, J. T.; Jasinski, J. B.; Achilefu, S. Fluorescence Manipulation by Gold Nanoparticles: From Complete Quenching to Extensive Enhancement. *J. Nanobiotechnol.* **2011**, *9*, 16.
- (28) Draine, B. T.; Flatau, P. J. Discrete-Dipole Approximation for Scattering Calculations. *J. Opt. Soc. Am. A* **1994**, *11* (4), 1491–1499.
- (29) Zhou, F.; Li, Z. Y.; Liu, Y.; Xia, Y. N. Quantitative Analysis of Dipole and Quadrupole Excitation in the Surface Plasmon Resonance of Metal Nanoparticles. *J. Phys. Chem. C* **2008**, *112* (51), 20233–20240.
- (30) Li, Z. Y.; Xia, Y. N. Metal Nanoparticles with Gain toward Single-Molecule Detection by Surface-Enhanced Raman Scattering. *Nano Lett.* **2010**, *10* (1), 243–249.
- (31) Ming, T.; Zhao, L.; Chen, H. J.; Woo, K. C.; Wang, J. F.; Lin, H. Q. Experimental Evidence of Plasmon-Directed Polarized Emission from Gold Nanorod-Fluorophore Hybrid Nanostructures. *Nano Lett.* **2011**, *11* (6), 2296–2303.
- (32) Chowdhury, M. H.; Pond, J.; Gray, S. K.; Lakowicz, J. R. Systematic Computational Study of the Effect of Silver Nanoparticle Dimers on the Coupled Emission from Nearby Fluorophores. *J. Phys. Chem. C* **2008**, *112* (30), 11236–11249.
- (33) Anger, P.; Bharadwaj, P.; Novotny, L. Enhancement and Quenching of Single-Molecule Fluorescence. *Phys. Rev. Lett.* **2006**, *96* (11), 113002.
- (34) Zhu, J.; Li, J. J.; Wang, A. Q.; Chen, Y.; Zhao, J. W. Fluorescence Quenching of Alpha-Fetoprotein by Gold Nanoparticles: Effect of Dielectric Shell on Non-Radiative Decay. *Nanoscale Res. Lett.* **2010**, *5* (9), 1496–1501.
- (35) Li, X.; Qian, J.; Jiang, L.; He, S. L. Fluorescence Quenching of Quantum Dots by Gold Nanorods and Its Application to DNA Detection. *Appl. Phys. Lett.* **2009**, *94* (6), 063111.
- (36) Qaradaghi, V.; Fathi, D. Two-Dimensional Analysis of Gold Nanoparticle Effects on Dye Molecule System. *Physica B* **2013**, *409*, 51–56.
- (37) Schneider, G.; Decher, G.; Nerambourg, N.; Praho, R.; Werts, M. H. V.; Blanchard-Desce, M. Distance-Dependent Fluorescence Quenching on Gold Nanoparticles Ensheathed with Layer-by-Layer Assembled Polyelectrolytes. *Nano Lett.* **2006**, *6* (3), 530–536.
- (38) Chen, J.; Jin, Y. H.; Fahrudin, N.; Zhao, J. X. Development of Gold Nanoparticle-Enhanced Fluorescent Nanocomposites. *Langmuir* **2013**, *29* (5), 1584–1591.
- (39) Zijlstra, P.; Chon, J. W. M.; Gu, M. Five-Dimensional Optical Recording Mediated by Surface Plasmons in Gold Nanorods. *Nature* **2009**, *459* (7245), 410–413.
- (40) Chang, W. S.; Ha, J. W.; Slaughter, L. S.; Link, S. Plasmonic Nanorod Absorbers As Orientation Sensors. *Proc. Natl. Acad. Sci. U.S.A.* **2010**, *107* (7), 2781–2786.
- (41) Liu, Q. K.; Cui, Y. X.; Gardner, D.; Li, X.; He, S. L.; Smalyukh, I. I. Self-Alignment of Plasmonic Gold Nanorods in Reconfigurable Anisotropic Fluids for Tunable Bulk Metamaterial Applications. *Nano Lett.* **2010**, *10* (4), 1347–1353.
- (42) Ling, L.; Guo, H. L.; Zhong, X. L.; Huang, L.; Li, J. F.; Gan, L.; Li, Z. Y. Manipulation of Gold Nanorods with Dual-Optical Tweezers for Surface Plasmon Resonance Control. *Nanotechnology* **2012**, *23*, 215302.
- (43) Muskens, O. L.; Giannini, V.; Sanchez-Gil, J. A.; Rivas, J. G. Strong Enhancement of the Radiative Decay Rate of Emitters by Single Plasmonic Nanoantennas. *Nano Lett.* **2007**, *7* (9), 2871–2875.
- (44) Kinkhabwala, A.; Yu, Z. F.; Fan, S. H.; Avlasevich, Y.; Mullen, K.; Moerner, W. E. Large Single-Molecule Fluorescence Enhance-

ments Produced by a Bowtie Nanoantenna. *Nat. Photonics* **2009**, *3* (11), 654–657.

(45) Bakker, R. M.; Drachev, V. P.; Liu, Z. T.; Yuan, H. K.; Pedersen, R. H.; Boltasseva, A.; Chen, J. J.; Irudayaraj, J.; Kildishev, A. V.; Shalaev, V. M. Nanoantenna Array-Induced Fluorescence Enhancement and Reduced Lifetimes. *New J. Phys.* **2008**, *10*, 125022.

(46) Vecchi, G.; Giannini, V.; Rivas, J. G. Shaping the Fluorescent Emission by Lattice Resonances in Plasmonic Crystals of Nanoantennas. *Phys. Rev. Lett.* **2009**, *102* (14), 146807.